

# Propagation of tightly bound excitons: a simple first-principles method of exciton kinetics

Chi-Cheng Lee (李啓正),<sup>1,2</sup> Xiaoqian M. Chen (陈小千),<sup>3</sup> Chen-Lin Yeh (葉承霖),<sup>1,4</sup> H. C. Hsueh (薛宏中),<sup>4</sup> Peter Abbamonte,<sup>3</sup> and Wei Ku (顧威)<sup>1,5</sup>

<sup>1</sup>*Condensed Matter Physics and Materials Science Department,  
Brookhaven National Laboratory, Upton, New York 11973, USA*

<sup>2</sup>*Institute of Physics, Academia Sinica, Nankang, Taipei 11529, Taiwan*

<sup>3</sup>*Department of Physics and Frederick Seitz Materials Research Laboratory, University of Illinois, Urbana, IL 61801, USA*

<sup>4</sup>*Department of Physics, Tamkang University, Tamsui, Taipei 25137, Taiwan*

<sup>5</sup>*Physics Department, State University of New York, Stony Brook, New York 11790, USA*

(Dated: March 4, 2013)

A simple first-principles method is proposed to describe propagation of tightly bound excitons via its kinetic kernel. By viewing the exciton as a composite object (internally consisting of local particle and hole in Wannier orbitals), the corresponding kinetic kernel encapsulates the detailed information of the propagation and decay of the exciton, applicable for all binding energies. Case study of LiF gives three branches of exciton dispersion, which we verified via inelastic X-ray scattering. The proposed real-space picture not only offers computationally inexpensive access to the full exciton dynamics, suitable even in the presence of surfaces and impurity scattering, but also provides intuitive physical understanding necessary for the optimization of exciton propagation in semiconductors, their nanostructures, and strongly correlated oxides.

PACS numbers: 71.15.Qe, 71.35.-y, 78.20.Bh, 78.47.-p

Exciton, a low-energy charge excitation involving a bound particle-hole pair, is one of the most utilized excitation of materials in practical applications. It plays important roles in many semiconductor applications, for example, in photovoltaic and other PN-junctions related devices [1–6]. One essential issue in real applications is the efficiency of the propagation of excitons and the associated decay / recombination processes [1–6]. Currently, excitons are typically studied via perturbation theory (so-called Bethe-Salpeter equation) [7–11], or via specially tuned approximation within the time-dependent density functional theory [11–14]. Particularly, nonimmune to the high computational expense, the emphasis has been only on the excitonic spectrum in the optical limit, most relevant to the creation of zero-momentum exciton, leaving the essential issues of exciton propagation mostly unaddressed.

The recent advances in X-ray scattering that allows mapping out the full momentum-energy dispersion of the excitons [15] further highlights the need to have a computationally inexpensive method, not only to describe the exciton propagation, but also to give an intuitive physical picture and a deeper understanding. This is particularly so given that more and more of the potential functional materials make use of the strongly correlated nature of the electrons, which require treatment of the many-body problem beyond the scope of perturbation theory. It is thus important and timely to develop a first-principles theory targeting specifically the exciton propagation.

In this letter, we propose a general approach that focuses on the essence of the kinetics of exciton. By integrating out the higher-energy virtual pair-breaking pro-

cesses, the exciton can be treated as a single composite object, instead of a particle-hole pair, and its kinetics can then be formulated in real-space via an excitonic kinetic kernel that serves the role similar to the hopping integral. In addition, the kinetic kernel encapsulates the information of exciton decay process and the necessary energy dependence to react to all binding energies. For systems where excitonic effect is large, namely the binding of exciton is strong, this real-space description, together with the reduction of the problem from two-body to one-body, is significantly more efficient for computation (easily by several orders of magnitude). In addition, the separation of non-local kinetic from the local interacting problem allows an accurate treatment of the local many-body problem. Taking the well known LiF as a case study, our results give three branches of excitons, which we verified experimentally via inelastic X-ray scattering. The proposed approach offers a simple and intuitive physical picture easily applicable to systems with surfaces (or other boundary conditions), impurity scattering, or strong many-body interactions. Therefore, it should facilitate greatly understanding of exciton propagation in all semiconductors, their nanostructures, and numerous strongly correlated functional materials.

The general idea of our approach is to use local excitons as real space basis and encapsulate their propagation into an excitonic kinetic kernel, similar to the hopping integral. This real-space approach makes sense because binding of the particle and hole is only significant in short range and thus the size of the exciton with practically relevant binding should be reasonably small. To this end, one needs to 1) define a “local” region, in which the local

excitons would be treated accurately enough, and 2) construct the kinetic kernel of the local excitons which gives a physical understanding of the exciton propagation and allows an inexpensive computation of the exciton spectrum in the full momentum / energy phase space. As a bonus, the separation of the kinetic processes from the local interacting problem would also allow a more accurate treatment of the local many-body physics. The first step is strongly case dependent, in both the physical size of the local region and the required proper treatment of local interaction (e.g.: local multiplets in strongly correlated materials). The case study of LiF below gives a detailed example of this step. The second step, on the other hand, is quite generic and will be the focus of this study.

Let's define the excitonic kinetic kernel  $T$  through the one-body equation of motion of the exciton (in matrix notation)

$$L[H] = L[H_L] + L[H_L]TL[H], \quad (1)$$

given the particle-hole correlation function  $L$  corresponding to the local Hamiltonian  $H_L$ , and the full Hamiltonian  $H$  with additional coupling beyond the local region. Note that the excitonic degree of freedom  $b_{\mathbf{R}N}^\dagger$ , as a basis for  $L_{\mathbf{R}N,\mathbf{R}'N'}$  and  $T_{\mathbf{R}N,\mathbf{R}'N'}$ , is defined in the direct product space of the particle  $p$  and hole  $h$  orbitals at the *same* local region indexed by  $\mathbf{R}$ :  $b_{\mathbf{R}N}^\dagger = c_{\mathbf{R}p}^\dagger c_{\mathbf{R}h}$ , since only strongly bound excitons smaller than the local region are of interest. Eq. 1 makes the physical interpretation of  $T$  obvious:  $T$  is the kernel responsible for the propagation (present in  $L[H]$ ) of local excitations (given by  $L[H_L]$ ).

This rigorous definition becomes practically useful with the simplification:

$$\begin{aligned} T &\equiv L^{-1}[H_L] - L^{-1}[H] \\ &= (L_0^{-1}[G[H_L]] - I[H_L]) - (L_0^{-1}[G[H]] - I[H]) \quad (2) \\ &\cong L_0^{-1}[G[H_L]] - L_0^{-1}[G[H]]. \end{aligned}$$

Here  $L_0(\mathbf{R}N, \mathbf{R}'N'; t, t') = G(\mathbf{R}p, \mathbf{R}'p'; t, t') * G(\mathbf{R}'h', \mathbf{R}h; t', t)$  is the “bare bubble” without interaction (vertex) at the two-particle level (even though it does contain the fully interacting  $G[H]$ .) This simplification of the exciton self-energy  $I[H]$  by its local counterpart  $I[H_L]$  is similar to that previously employed with the dynamical mean field approximation [16]. It is physically reasonable because of the general short-range nature of the self-energy. Particularly, at the lowest order approximation of  $I$ , employed in practically all first-principles solution of the Bethe-Salpeter equation,  $I[H] = I[H_L]$  and this simplification is exact. Once  $T$  is obtained from Eq. 2, the full spectrum of  $L[H]$  can be obtained effortlessly from Eq. 1, with several orders less computation effort than the two-body Bethe-Salpeter equation (BSE).

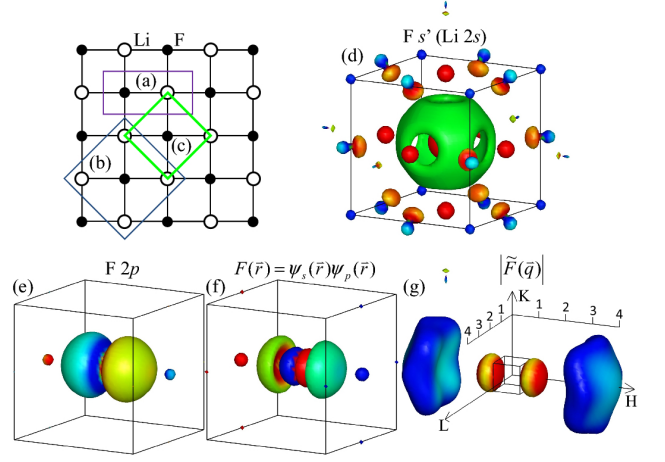


FIG. 1: (color online). Three ways to define local regions via unit cells respecting to (a) translational symmetry, (b) rotational symmetry, and (c) both translational and rotational symmetries. Following (c), an effective F- $s'$  Wannier orbital (d) composed of symmetric superposition of Li 2s orbitals is compared to a F 2p Wannier orbital (e). (f) Shape of the exciton from product of Li 2s and F 2p gives the form factor (g) in momentum space. Boxes denote the conventional unit cell in (d), (e), and (f), and the corresponding 1st Brillouin zone in (g).

We now use the prototypical LiF to demonstrate the simple method and the deep insights it can offer. Crystal LiF has a simple NaCl structure with ionic electronic structure, with a 14.2 eV band gap [17] defined by occupied F  $p$  bands and a unoccupied Li  $s$  band. The physics of excitons in LiF is thus dominated by these low-energy bands. Furthermore, the strong ionicity of the system implies a dominating short-range attraction between a hole in the F  $p$  orbitals and a particle in the nearest neighboring Li  $s$  orbital. We will therefore define a local region containing only one F for simplicity. The straightforward choice is a small unit cell containing one F and one Li, as illustrated in Fig. 1(a). This choice, however, does not build in the rotational symmetry in the local region. Fig. 1(b) gives an alternative choice often employed in the cluster model [18]. While including the rotational symmetry, the local Hilbert space is, however, overcomplete in that one F is paired with four Li (actually six Li in 3D), and thus cannot be used to build a crystal under translational symmetry. Fig. 1(c) gives the best choice of the local region, which contains one F and effectively one Li from combining all its neighboring sites. This choice respects both the translational and rotational symmetries of the system and is thus ideal for the physical description.

In practice, the low-energy Hilbert space of such a local region can be constructed by making use of the gauge freedom of the Wannier function [19, 20]. Fig. 1(d) shows the resulting Li  $s$  Wannier orbital centered at the F site, as a symmetric superposition of atomic  $s$  orbitals. Recall

a similar construction [21] in the well-known Zhang-Rice singlet in the cuprate. Effectively, the local region is just a “super F atom” containing three  $p$  orbital (cf: Fig. 1(e)) and one  $s'$  orbital [15] in a simple fcc lattice, and the tightly bound excitons can now be viewed effectively as intra-“atomic” Frenkel excitons. The excitonic Hilbert space  $N$  is then simply spanned by three local excitons made of a particle in  $s'$  orbital and a hole in  $p_x$ ,  $p_y$ , or  $p_z$  orbital. Fig. 1(f) also demonstrates the probability amplitude of the exciton in real space, obtained from the product of the particle and hole orbitals [22].

With the local Hilbert space defined, excitonic kinetic kernel can be easily computed via Eq. 2. As a simple illustration, the fully dressed Green’s function is obtained approximately from self-consistent DFT Hamiltonian with a +5 eV shift in the on-site energy of  $s'$  orbital to counter the self-interaction error. The corresponding band structure contains a 14.2 eV band gap, consistent with the GW calculation [17, 23]. We then compute the corresponding  $L_0[H_L]$  and  $L_0[H]$  from the standard convolution [24] in Wannier function basis. The resulting  $L_0[H_L]$  contains trivially a pole at  $\omega_0 = \omega_p - \omega_h = 21.9$  eV, corresponding to the energy difference between the particle and the hole. (Since all three “bare” excitons are symmetry related,  $L_0[H_L]$  is diagonal and  $N$  independent.) Turning on the local binding interaction of  $U_B \sim \int dx dx' V_{sp}(x, x') n_s(x) n_p(x') \sim 7$  eV simply lowers the pole to  $\omega_{exciton} = \omega_0 - U_B = 14.9$  eV in  $L[H_L]$  (ignoring the fine multiplet splitting.) Note that our  $U_B$  is with respect to the binding energy of local bare exciton and is thus much larger than the binding energy between Bloch-like orbitals, typically referred in the context of Wannier exciton.

As shown in Fig. 2, the resulting excitonic kinetic kernel obtained from Eq. 2 contains several interesting characteristic features. First, the kinetic kernel is strongly energy dependent. This is physically necessary because  $T$  needs to generate the correct  $U_B$ -dependent kinetics of excitons *without* the knowledge of  $U_B$  to be introduced in  $L[H_L]$ . Particularly,  $T$  hosts a  $1/(\omega - \omega_0) = 1/U_B$  decay in all its components. Since  $T$  is like the hopping integral, this indicates a heavier mass (reduced hopping) for excitons with stronger binding (lower energy). This is the exact behavior in the strong coupling limit, in which the exciton can only propagate by virtually moving the particle first (paying the binding energy  $U_B$  in the intermediate state,) followed by the hole (to reform the pair), a 2nd order process giving  $T \sim 2t_p t_h / U_B \propto 1/U_B$ . (Here  $t_p/t_h$  refers to the hopping of the particle/hole.)

Second, the kinetic kernel has imaginary part spanning over a wide energy range, representing excitonic decaying channels. In fact, the energy span of the imaginary part is exactly that of the Landau continuum from unbound excitations. This is not surprising because plugging  $L[H_L]$  with unbound excitons ( $U_B = 0$  and  $L[H_L] = L_0[H_L]$ ) into Eq. 1 must, by construction, recover exactly the

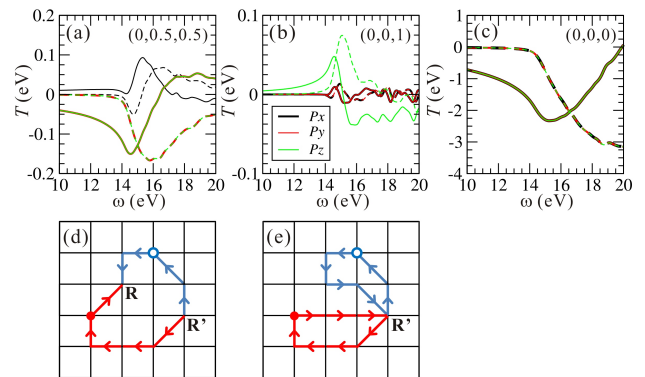


FIG. 2: (color online). The real (solid lines) and imaginary (dashed lines) parts of two-particle kinetic kernel  $T(\mathbf{R}N, \mathbf{R}'N)$  for (a)  $\mathbf{R}' - \mathbf{R} = (0, 0.5, 0.5)$ , (b)  $\mathbf{R}' - \mathbf{R} = (0, 0, 1)$ , and (c)  $\mathbf{R}' - \mathbf{R} = (0, 0, 0)$  for  $N = p_x, p_y$ , and  $p_z$ . Virtual processes integrated in off-site (d) and on-site (e) components of  $T$ .

TABLE I:  $\text{Re}T(\mathbf{R}N, \mathbf{R}'N); \tilde{\omega}_{exciton} = 13.4$  eV in meV.

$\mathbf{R}' - \mathbf{R}$	(0,0.5,0.5)			(0,0,1)		
	$p_x$	$p_y$	$p_z$	$p_x$	$p_y$	$p_z$
$p_x$	12.2	0	0	0	0	0
$p_y$	0	-88.8	-89.4	0	0	0
$p_z$	0	-89.4	-88.8	0	0	17.3

Landau continuum in the resulting  $L[H] = L_0[H]$ , and the information of the continuum can only come from  $T$ . ( $L_0[H_L]$  has no knowledge of the dispersion.) Physically, this reflects the fact that the definition of  $T_{\mathbf{R}N, \mathbf{R}'N'}$  via Eq. 1 integrates out all the virtual processes with unbound particle and hole traveling independently from  $\mathbf{R}'$  to  $\mathbf{R}$ , as demonstrated in Fig. 2 (d). Therefore, the  $T$  describes the exciton kinetics exactly not only in the strong binding limit, but also in the weak binding limit.

Third, the kinetic kernel has a significant negative diagonal elements [c.f. Fig. 2(c)] that reduces the local exciton energy to  $\tilde{\omega}_{exciton} \sim 13.4$  eV (estimated from  $\omega - \omega_{exciton} - \text{Re}T_{0N, 0N}(\omega) = 0$ .) This renormalized exciton energy represents the average energy of the propagating exciton in the crystal. It is important to distinguish this renormalization from the binding of local exciton, as it originates from virtual kinetic processes illustrated in Fig. 2(e). For large  $U_B$ , the lowest order of such processes would give  $T \sim -(t_p^2 + t_h^2)/U_B$  for each of the 12 possible intermediate de-paired states in the FCC lattice.

Before computing the full  $L$  from Eq. 1, let’s first examine the physical insights  $\text{Re} T$  offers, by considering it as an effective hopping integral (c.f. Table I). Regarding  $\tilde{\omega}_{exciton}$  and  $\text{Re} T_{\mathbf{R}, \mathbf{R}' \neq \mathbf{R}}(\tilde{\omega}_{exciton})$  as diagonal and off-diagonal elements, a simple diagonalization gives an estimated exciton dispersion containing three exciton bands shown in Fig. 3(a). Notice a striking similarity of the

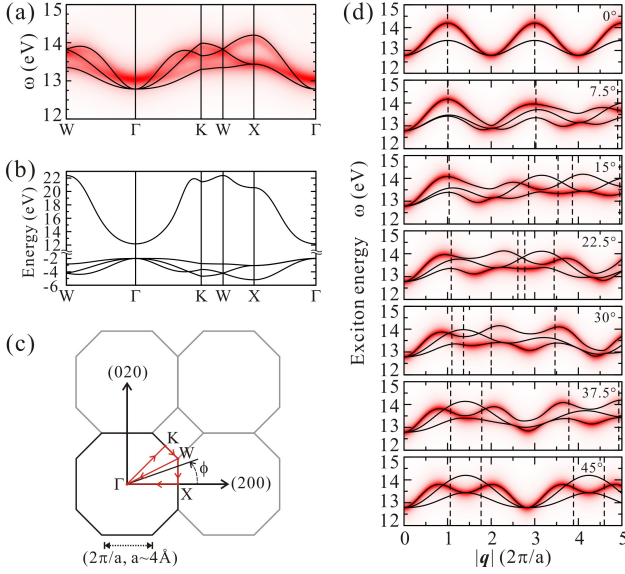


FIG. 3: (color online). (a) Exciton dispersion from diagonalizing  $\text{Re}T(\omega = 13.4 \text{ eV})$  (solid curves), compared to  $L(\mathbf{q})$  colored by red. (b) Band structure of Wannier orbital for Li  $s$  ( $E > 0$ ) and F  $p$  ( $E < 0$ ). (c) Selected  $k$  paths on the  $xy$  plane, denoted by  $\phi$ . (d) Exciton dispersion along selected paths, with the longitudinal component colored in red. Dashed lines denote the zone boundaries in (c).

dispersion to that of the F- $p$  bands in Fig. 3(b), beside a smaller bandwidth. This is understandable since the excitons here have the same symmetry properties as the F- $p$  orbitals [c.f. Fig. 1(e) and (f)], thanks to the zero angular momentum of the F- $s'$  orbital. Consequently,  $T \sim 2(t_p/U_B)t_h$  simply resembles  $t_h$  with a  $2t_p/U_B$  reduction that wipes out all longer range hoppings. (The comparison appears up-side-down because  $t_p < 0$ .) Obviously, the standard effective mass description [25, 26] of Wannier exciton propagation is seriously inadequate here. In essence, the exciton binding always enhances the tight-binding nature of the excitons, making them propagate more like Frenkel excitons.

Next, the complete description of exciton propagation and decay are computed from inserting  $T$  into Eq. 1. Indeed the resulting dispersion is quite close to the above simple estimation except: 1) Near the bottom of the exciton bands around  $\Gamma$  point, the actual dispersion is weaker than the estimation, due to the above mentioned decay of  $T(\omega)$  at lower energy. 2) Near the top of the exciton bands, the exciton peak is physically broadened, reflecting a shorter lifetime from decaying into the Landau continuum encapsulated in  $\text{Im}T$ .

Our results of exciton propagation leads to an exciting realization that all three branches of the excitons can be observed via inelastic X-ray scattering. Fig. 3(d) shows the exciton bands along different paths in the Brillouin zone, weighted by their longitudinal ( $\parallel \mathbf{q}$ ) contribution. Typically, one would expect that out of the three

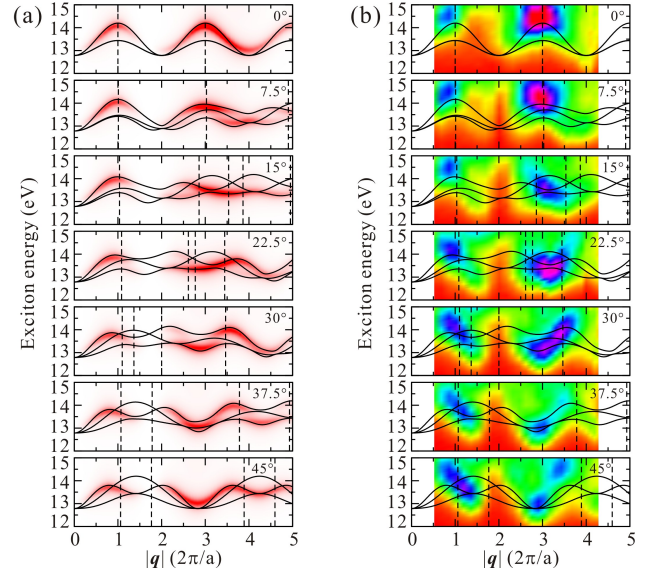


FIG. 4: (color online). (a) Imaginary part of dynamical linear response function  $\chi$  in selected directions (c.f.:Fig. 3), together with exciton dispersion from  $\text{Re}T$  at  $\omega = 13.4 \text{ eV}$  (solid curves). The theoretical intensity for  $q \leq 1.5$  is reduced by 2.6 to mimic screening by the plasmon pole. (b) Exciton dispersion measured by inelastic X-ray scattering in the same directions.

branches of the exciton, only the longitudinal mode can be observed experimentally, given the X-ray matrix element  $M_N^{\mathbf{q}} = \int d\mathbf{x} \exp^{-i\mathbf{q}\cdot\mathbf{x}} \langle \mathbf{x} | \mathbf{0}p \rangle \langle \mathbf{0}h | \mathbf{x} \rangle$  [22]. However, because of the zone folding, hybridization with transverse modes becomes significant near the zone boundaries in most off-high-symmetry directions. Consequently, the transverse modes receive significant spectral weight outside the first zone, allowing direct experimental observation of all three branches of excitons.

We verify the theoretical results by performing inelastic X-ray scattering along different directions between (100) and (110) [24]. Indeed, the measured spectra show good agreement with the theoretical response function,  $\chi(\mathbf{q}, \omega) = \sum_{NN'} M_N(\mathbf{q}) L_{NN'}(\mathbf{q}) M_{N'}^*(\mathbf{q})$ , despite the resolution-related broadening of the experimental data. (A spectral weight reduction for  $q \leq 1.5$  due to plasmon screening is included in  $L$  via additional Hartree contribution [27]. This improves the agreement in the spectral weight, but has little effects on the exciton dispersion of interest here.) As soon as  $\mathbf{q}$  deviates from the high-symmetry direction, a clear “break” in the dispersion is observed, for example at  $q \sim 3.5(2\pi/a)$  for  $\theta = 7.5^\circ$  and at  $q \sim 4(2\pi/a)$  for  $37.5^\circ$ , which actually corresponding to switching from one exciton band to another, as indicated in the theoretical results.

Finally, several important aspects of our method is worth mentioning. First, the separation of the non-local kinetics from the local binding of exciton in our framework allows a more accurate many-body treatment of the

local excitation in  $L[H_L]$  (say via exact diagonalization or quantum Monte Carlo) before solving Eq. 1. This is particularly important in strongly correlated systems, in which local interaction is strong enough to induce significant multiplet splitting [27]. Furthermore, such separation of the problem significantly reduces the computational expense of exciton dynamics, as the proposed evaluation of excitonic kinetic kernel  $T$  is purely non-interacting, while the potentially expensive interacting problem is only local. On top of that, our use of Wannier function as basis, and the implicit projection of non-local particle-hole pair from our formulation further reduce the computation greatly. We estimate that our method is at least several orders of magnitude cheaper than the standard Bethe-Salpeter equation where a  $\sim 10^8$  matrix elements of the electron-hole interaction [23] are needed in comparison with  $\sim 10^4$  matrix elements. A similar reduction (by  $\sim 2$  orders of magnitude) is achieved in the matrix elements of the form factor of the experimental probe. Finally, the real-space formulation employed in this study is particularly suitable in treating exciton scattering from surfaces, impurities, or other boundary conditions. All together, these significant advances make this method ideal for future studies of exciton propagation and decay in modern functional materials, like doped semiconductors and strongly correlated transition metal oxides, as well as their nano-structures, thin films, and heterogeneous interfaces.

In summary, we propose a new real-space theoretical framework to describe the propagation and decay of tightly bound excitons. By explicitly integrating out the intermediate de-pairing processes, a simple one-particle description of exciton is given by the effective exciton kinetic kernel, which gives intuitive physical picture of both mass enhancement and decay into unpaired particle and hole. The proposed method is exact in both weak and strong binding limit. Furthermore, the separation of non-local kinetic from the local binding of excitons allows a more accurate treatment of local many-body problem beyond perturbation theory, particularly necessary for strongly correlated materials. Together with the Wannier function approach, the method is computationally much more affordable than the standard two-particle Bethe-Salpeter equation method, by easily several orders of magnitude. In the prototypical LiF, our theory predicted three exciton bands that can be measured experimentally over a large momentum. We verify this via inelastic X-ray scattering and found good agreement. Our real-space approach can incorporate straightforwardly scattering via impurities or boundary conditions, and thus will find broad applications in the study of nano-structures, thin films or surfaces of semi-conductors and strongly correlated Mott insulators.

Theoretical work is supported by the U.S. Department of Energy (DOE), Office of Basic Energy Science, under Contract No. DE-AC02-98CH10886 and DOE CMSN.

IXS measurements are supported by Department of Energy (DOE) grant DE-FG02-07ER46459. Use of the Advanced Photon Source is supported by DOE Contract DE-AC02-06CH11357. C.-C. Lee thanks useful discussions with T.-K. Lee and the support by the National Science Council (NSC) in Taiwan. C.-L. Yeh acknowledges the support by NSC of Taiwan and the Research Abroad Program. C.-C. Lee and H. C. Hsueh acknowledge National Center for High-performance Computing of Taiwan for CPU time. H. C. Hsueh also thanks the NSC and NCTS of Taiwan for support.

\* email: weiku@bnl.gov (theory) and abbamonte@mrl.illinois.edu (experiment)

- 
- [1] M. H. Huang, S. Mao, H. Feick, H. Yan, Y. Wu, H. Kind, E. Weber, R. Russo, and R. Yang, *Science* **292**, 1897 (2001).
  - [2] S. Koizumi, K. Watanabe, M. Hasegawa, and H. Kanda, *Science* **292**, 1899 (2001).
  - [3] J. B. Sambur, T. Novet, and B. A. Parkinson, *Science* **330**, 63 (2010).
  - [4] V. K. Thorsmølle et al., *Phys. Rev. Lett.* **102**, 017401 (2009).
  - [5] J. Tsutsumi et al., *Phys. Rev. Lett.* **105**, 226601 (2010).
  - [6] F. Deschler et al., *Phys. Rev. Lett.* **107**, 127402 (2011).
  - [7] G. Onida et al., *Phys. Rev. Lett.* **75**, 818 (1995).
  - [8] M. Rohlfing and S. G. Louie, *Phys. Rev. Lett.* **81**, 2312 (1998).
  - [9] L. X. Benedict et al., *Phys. Rev. Lett.* **80**, 4514 (1998).
  - [10] H. C. Hsueh, G. Y. Guo, and S. G. Louie, *Phys. Rev. B* **84**, 085404 (2011).
  - [11] G. Onida et al., *Rev. Mod. Phys.* **74**, 601 (2002).
  - [12] R. Bauernschmitt and R. Ahlrichs, *Chem. Phys. Lett.* **256**, 454 (1996).
  - [13] L. Reining et al., *Phys. Rev. Lett.* **88**, 066404 (2002).
  - [14] A. Marini, R. D. Sole, and A. Rubio, *Phys. Rev. Lett.* **91**, 256402 (2003).
  - [15] P. Abbamonte et al., *PNAS* **105**, 12159 (2008).
  - [16] T. Maier, M. Jarrell, T. Pruschke, and J. Keller, *Phys. Rev. Lett.* **85**, 1524 (2000).
  - [17] E. L. Shirley, L. J. Terminello, J. E. Klepeis, and F. J. Himpsel, *Phys. Rev. B* **53**, 10296 (1996), and references therein.
  - [18] M. W. Haverkort et al., *Phys. Rev. Lett.* **99**, 257401 (2007).
  - [19] N. Marzari and D. Vanderbilt, *Phys. Rev. B* **56**, 12847 (1997).
  - [20] W. Ku et al., *Phys. Rev. Lett.* **89**, 167204 (2002).
  - [21] W.-G. Yin and W. Ku, *Phys. Rev. B* **79**, 214512 (2009).
  - [22] B. C. Larson et al., *Phys. Rev. Lett.* **99**, 026401 (2007).
  - [23] M. Rohlfing and S. G. Louie, *Phys. Rev. B* **62**, 4927 (2000).
  - [24] See EPAPS Document No. for the details of IXS experiment and computational parameters.
  - [25] L. E. Brus, *J. Chem. Phys.* **80**, 4403 (1984).
  - [26] V. M. Agranovich, *Excitations in Organic Solids* (Oxford University Press, 2009).
  - [27] C.-C. Lee, H. C. Hsueh, and W. Ku, *Phys. Rev. B* **82**, 081106 (2010).